AGU PUBLICATIONS

JGR

Journal of Geophysical Research: Atmospheres

RESEARCH ARTICLE
10.1002/2017JD027286

Key Points:
- The temporal variation in the CCN activity of $PM_{1.0}$ is linked to changes in the chemical composition and mixing state at a suburban site
- The WSOM/sulfate ratios were linked to a hygroscopicity parameter in the accumulation size
- Hygroscopicity of particles with the Aitken mode size is controlled by the EC concentration

Supporting Information:
- Supporting Information S1
- Data S1

Correspondence to:
Y. Miyazaki,
yuzom@lowtem.hokudai.ac.jp

Citation:
Müller, A., Y. Miyazaki, S. G. Aggarwal, Y. Kitamori, S. K. R. Boreddy, and K. Kawamura (2017), Effects of chemical composition and mixing state on size-resolved hygroscopicity and cloud condensation nuclei activity of submicron aerosols at a suburban site in northern Japan in summer, *J. Geophys. Res. Atmos.*, *122*, 9301–9318, doi:10.1002/2017JD027286.

Received 12 JUN 2017
Accepted 9 AUG 2017
Accepted article online 14 AUG 2017
Published online 4 SEP 2017

Effects of chemical composition and mixing state on size-resolved hygroscopicity and cloud condensation nuclei activity of submicron aerosols at a suburban site in northern Japan in summer

Astrid Müller[1,2], Yuzo Miyazaki[1], Shankar G. Aggarwal[1,3], Yasuyuki Kitamori[1], Suresh K. R. Boreddy[1], and Kimitaka Kawamura[1,4]

[1]Institute of Low Temperature Science, Hokkaido University, Sapporo, Japan, [2]Graduate School of Environmental Science, Hokkaido University, Sapporo, Japan, [3]CSIR-National Physical Laboratory, New Delhi, India, [4]Now at Chubu Institute for Advanced Studies, Chubu University, Kasugai, Japan

Abstract Ambient hygroscopic properties, numbers of size-segregated cloud condensation nuclei (CCN) at different supersaturations (0.1%–0.8%), and the chemical composition of submicron particles were simultaneously measured at a suburban site in northern Japan in summer. Two distinct periods with different growth factors (GF), CCN activation diameters, and chemical compositions were observed. The data suggest that internally mixed sulfate aerosols dominated the accumulation size mode in relatively aged aerosols during the first period, whereas particles observed during the latter periods showed external mixing dominated by organics, which was linked to low hygroscopicity and CCN activity. In particular, the higher loading of water-soluble organic matter (WSOM; ~60% of OM by mass) with increased WSOM/sulfate ratios corresponded to a low hygroscopicity parameter derived from the CCN measurement ($\kappa_{CCN} = 0.15 \pm 0.02$) at a dry diameter ($D_{dry}$) of 146 nm. The results suggest that WSOM, likely dominated by the influence of biogenic sources, contributed to reducing the hygroscopicity and CCN activation at this particle size. Temporal variations in the number concentrations for low GF mode at $D_{dry} = 49.6$ nm were similar to those in the elemental carbon (EC) concentration, suggesting that EC contributed to reducing hygroscopicity at this smaller size. Our results suggest that chemical composition and mixing state are important factors controlling the hygroscopicity and CCN activation of submicron particles. These results provide useful data sets of size-resolved subsaturated and supersaturated hygroscopicity and highlight the importance of the abundance of OM relative to sulfate in predicting the effects on climate change.

1. Introduction

Atmospheric aerosol particles play an important role in controlling the radiative forcing of the Earth, both directly by absorbing and scattering radiation, and indirectly by acting as cloud condensation nuclei (CCN) and ice nuclei (IN). Although the effects of aerosols on the properties of clouds are important in understanding climate change, the aerosol-cloud interaction is highly uncertain [*Intergovernmental Panel on Climate Change*, 2013]. Activation of CCN to form cloud droplets is controlled by the number concentration, sizes, and mixing state of chemical species in aerosol particles [e.g., *McFiggans et al.*, 2006; *Farmer et al.*, 2015]. *Dusek et al.* [2006] suggested that CCN activation primarily depends on particle sizes, whereas *Burkart et al.* [2011] showed that the complexity in externally and internally mixed aerosols prevents us from accurately predicting CCN activation from the size distributions alone.

Among the chemical and physical properties of particles, solubility and hygroscopicity play important roles in the complex aerosol-cloud interaction [*McFiggans et al.*, 2006; *Lee et al.*, 2010]. κ-Köhler theory parameterizes the solute contribution in terms of a single hygroscopicity parameter, κ [*Petters and Kreidenweis*, 2007]. κ represents a scaled volume fraction of soluble material in particles and provides a theoretical framework to derive bulk hygroscopicity for particles with internal mixtures. The complexity of aerosol composition, particularly for the organic fraction, prevents atmospheric models from accurately depicting the aerosol-cloud interaction. Sulfate is one of the most effective aerosol components to be activated as CCN [*Seinfeld and Pandis*, 2006; *Sun and Ariya*, 2006]. By contrast, organics generally have lower κ values between 0 and 0.1 [*Petters and Kreidenweis*, 2007; *Duplissy et al.*, 2011] for primary emitted compounds. Atmospheric aging and the formation of secondary organic aerosols (SOA) can change the CCN activity. This is typically

attributable to changes in the surface composition of particles by heterogeneous oxidation and the resulting changes in the particle's ability to uptake water.

Previous studies reported that the bulk value of κ for SOA ranges between ~0 and ~0.4 [*Engelhart et al.*, 2008]; these values likely represent the volume-weighted average of a broader range of constituent κ values [*Suda et al.*, 2012]. For example, the oxidation products of 3-methylfuran with OH in the presence of NO_x have a κ = 0.06 [*Suda et al.*, 2012], whereas κ values reported for SOA derived from monoterpene and isoprene are 0.10–0.15 [*Prenni et al.*, 2007; *Engelhart et al.*, 2008] and 0.10–0.12 [*King et al.*, 2010; *Engelhart et al.*, 2011], respectively.

Atmospheric processing of aerosols depends on various chemical and physical reactions in the atmosphere as well as differences in their origin and transport processes. Understanding how such processes lead to changes in the particle size and particle chemical composition, and how they are interrelated, is important to accurately reproduce the global distributions of CCN and their impacts on climate change. Due to the complexity of the atmospheric processing, time-resolved field measurements relating CCN activity to hygroscopicity and chemical composition have been extensively conducted in previous studies [*Fors et al.*, 2011; *Jurányi et al.*, 2011; *Sihto et al.*, 2011; *Silvergren et al.*, 2014; *Kawana et al.*, 2016]. However, field studies on the hygroscopicity and cloud forming properties of atmospheric particles affected by both anthropogenic and biogenic sources are limited.

In this study, we aim to understand the characteristics of aerosol composition in a suburban area, and the impact of aerosol composition on both subsaturated and supersaturated particle hygroscopicity. Simultaneous measurements of size-resolved CCN concentrations, hygroscopic growth, particle size distributions, and chemical composition in submicron aerosols were made at a suburban site in northern Japan in the summer of 2008. In spite of the suburban environment, our observational site has been suggested to be largely influenced by biogenic sources in addition to anthropogenic sources, especially in summer [*Pavuluri et al.*, 2013]. Therefore, our site provides unique opportunities to investigate the effects of inhomogeneity of sources and aerosol aging on CCN activity. The current study discusses the relevance of the aerosol mixing state, chemical composition, and different possible sources.

2. Experiments

2.1. Measurement Site

Figure 1 shows the location of the measurement site and the surrounding area. The site is located at the campus of Hokkaido University (43°3′56″N and 141°21′27″E) at the north of the downtown area of Sapporo, northern Japan. The study site, which belongs to the cool temperate zone, is surrounded by vegetation and residential areas. Urban industrial areas are located to the south and east, whereas vegetation and residential areas are located to the west and northwest of the sampling site.

Ambient aerosol measurements were carried out during the period of 1 to 17 July 2008. Our previous field studies suggested that in summer, both isoprene-derived and α-pinene-derived SOA similarly contribute to the production of the water-soluble organic carbon (WSOC) mass in aerosols at the same site and at a nearby forest site [*Miyazaki et al.*, 2012; *Pavuluri et al.*, 2013]. Consequently, similar contributions of isoprene and α-pinene emissions are expected to affect ambient aerosols at this site in summer. During the study period, the average temperature was 21.0°C ± 2.7°C, while precipitation was only observed on 11 July. The ambient aerosols were sampled through a $PM_{1.0}$ cyclone inlet. The sampled aerosols were then introduced to each online instrument as explained below.

2.2. CCN and Particle Number Size Distribution

Figure 2 shows the instrument setup for the measurements of the CCN, hygroscopic growth factors (GF) measured with a hygroscopicity tandem differential mobility analyzer (HTDMA), and particle size distributions. Ambient aerosol particles ($PM_{1.0}$) were dried at relative humidity (RH) $<$ 5% with two diffusion dryers filled with silica gel and a molecular sieve. Number concentrations of CCN (N_{CCN}) were measured as a function of dry diameter (D_{dry}, RH $<$ 5%) and supersaturation using a continuous-flow thermal-gradient cloud condensation nuclei counter (CCNC-100: Droplet Measurement Technologies) [*Roberts and Nenes*, 2005]. The CCN counter was operated in parallel with a condensation nuclei (CN) counter (CPC 1; TSI, Model 3010) downstream of a differential mobility analyzer (DMA 1: TSI Model 3081) (Figure 2) to obtain the total particle

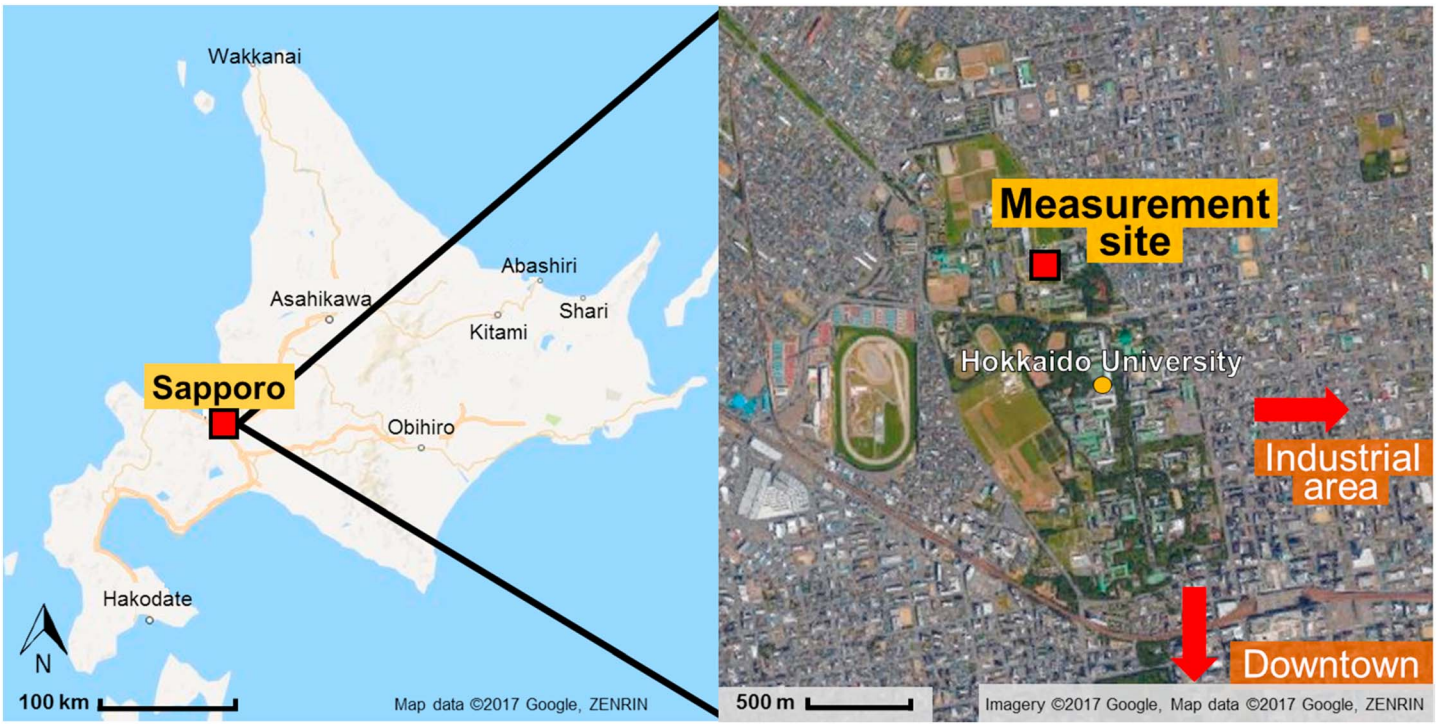

Figure 1. Location of the measurement site at north campus of Hokkaido University, Sapporo, northern Japan (43°3′56″N and 141°21′27″E) (copyright Google Inc.).

number concentration (N_{CN}). The total flow rate of air into the CCN counter was 0.5 L min^{-1} with the ratio of sheath to sample flows of ~10. The CCN counter was stepped through four different column temperature gradients, which were calibrated to supersaturations (SS) of 0.10%, 0.30%, 0.50%, and 0.80%. The concentration of CCN was measured for particles with D_{dry} ranging from 20.2 to 429 nm for 1.5 h at each SS. The residence time of the particles in the column was ~10 s, which is sufficient for the particles to grow to droplets with diameters between 0.75 μm and 1 μm [*Paramonov et al.*, 2013]. Calibration of the CCN counter was performed using ammonium sulfate (AS). Each SS was measured three times for laboratory-generated AS, and the presented data are the averages of these measurements.

For the calibration using particles with identical size and chemical composition, the activation diameter of CCN is generally defined as D_{dry} at which N_{CCN} reaches 50% of the total particle number concentration (N_{CN}) at a certain supersaturation (SS) [e.g., *Rose et al.*, 2008]. Here the activation diameter of CCN for ambient particles is defined as D_{act}. The overall uncertainty of the N_{CCN}/N_{CN} ratio controlled by the counting efficiencies of the CPC and the optical particle counter (OPC) in the CCN counter was estimated to be less than 10%. The estimation of the uncertainty is based on the variation of the maximum ratios of the N_{CCN}/N_{CN} for the AS aerosols during the calibration. Once D_{act} at a certain SS is determined, the hygroscopicity parameter, κ_{CCN}, can be calculated for particles corresponding to that D_{dry} [*Petters and Kreidenweis*, 2007].

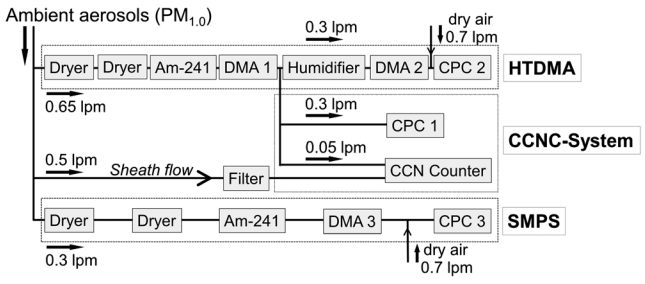

Figure 2. Schematic of the experimental setup for the HTDMA, CCNC, and SMPS.

$$\kappa(SS, D_{dry}) \approx \frac{4A^3}{27 D_{dry}^3 \ln^2\left(1 + \frac{SS}{100\%}\right)} \quad (1)$$

$$A = \frac{4 \sigma_{s/a} M_w}{R T \rho_w}, \quad (2)$$

where ρ_w is the density of water, M_w is the molar mass of water, $\sigma_{s/a}$ is the surface tension of the solution-air interface using the value of pure water ($\sigma_{s/a}$ = 0.072 J m^{-2}) to obtain a κ value in the standard state, R is

the universal gas constant, T is the absolute temperature (T = 298.15 K).

Particle size distributions were measured using a Scanning Mobility Particle Sizer (SMPS). After drying and single charging via an aerosol bipolar charger (AM-241), the particles were measured with DMA 3 and CPC 3 (TSI, Model 3022). The particle number dN/dlogd in the 64 channel per decade resolution was normalized by the total number (dN/dlogd/N_{TOTAL} (particle cm^{-3})).

2.3. Hygroscopic Growth Factor

The hygroscopic GF at 85% RH were measured with the HTDMA as a function of D_{dry} ranging from 24.1 to 359 nm. The hygroscopic GF is defined as the particle diameter at a given RH (D(RH)) divided by its D_{dry}:

$$\mathrm{GF(RH)} = \frac{D(\mathrm{RH})}{D_{\mathrm{dry}}} \tag{3}$$

The ambient aerosol particles ($PM_{1.0}$) were dried to RH $<$ 5% via two diffusion dryers as described in the previous subsection (Figure 2). The aerosols were then passed through the AM-241 to achieve single charged particles and classified by a differential mobility analyzer (DMA 1: TSI Model 3081). The particles were selected at 16 specific mobility diameters between 24.1 and 359 nm. Humidification of the particles at 85% ± 1% RH was performed using a humidity conditioner consisting of a Nafion tube. The RH was regulated by controlling the dried and humidified airflows into the tubing. The residence time of the particles between the inlet of the humidity conditioner and the DMA 2 was approximately 10 s [*Boreddy et al.*, 2014], which is considered to be sufficient for the particles to reach their equilibrium [*Chan and Chan*, 2005; *Duplissy et al.*, 2009]. The resulting number size distribution after humidification was measured using the second DMA (DMA 2) and the condensation particle counter (CPC 2). Calibration of the HTDMA system was made with AS. The measurement uncertainty for GF at 85% RH was ±1%, which is similar to that reported in previous studies using the same measurement system [*Aggarwal et al.*, 2007; *Jung et al.*, 2011; *Boreddy et al.*, 2014]. More details about the principle are described in previous studies [e.g., *Mochida et al.*, 2006].

Like the supersaturated hygroscopicity parameter (κ_{CCN}), κ values were also calculated using the GF data (κ_{GF}) [*Petters and Kreidenweis*, 2007], which relates the water activity to the dry particle volumes.

$$\kappa = \frac{\left(\mathrm{GF(RH)}^3 - 1\right)(1 - a_\omega)}{a_\omega} \tag{4}$$

$$a_\omega = \mathrm{RH}\left(\exp\left(\frac{4\,\sigma_{s/a}/M_w}{R\,T\,\rho_w\,\mathrm{GF(RH)}\,D_{\mathrm{dry}}}\right)\right)^{-1} \tag{5}$$

where α_ω is the water activity, ρ_w is the density of water, M_w is the molar mass of water, $\sigma_{s/a}$ is the surface tension of the solution-air interface using the value of pure water ($\sigma_{s/a}$ = 0.072 J m^{-2}) to obtain a κ value in the standard state, R is the universal gas constant, T is the absolute temperature, and D_{dry} the particle dry diameter. The comparison between κ_{GF} and κ_{CCN} values is discussed in section 3.2.

To calculate the fraction of the particle number concentration of the GF distributions, the *k*-means cluster analytical tool of the Igor Pro software (version 6.3.7.2) was used. The tool uses an iterative algorithm to classify the clustering of data into groups; hence, each data point belongs to a group of the closest mean value. It then calculates peaks of the number fractions of particles of the GF distributions, which is discussed in section 3.3.

2.4. Measurements of Aerosol Chemical Composition

Semicontinuous measurement of WSOC in $PM_{1.0}$ was made using a particle-into-liquid sampler (PILSs) coupled to a total organic carbon (TOC) analyzer (Model 810; Sievers, Boulder, CO) [*Miyazaki et al.*, 2006, 2012] in parallel with the measurements of GF and CCN. The details of the instrument are given elsewhere [*Miyazaki et al.*, 2006]. The inlet for the PILS was identical to that for the CCN and hygroscopicity measurements.

The mass concentrations of OC and EC were measured using a semicontinuous EC/OC analyzer (Sunset Laboratory Inc., Tigard, OR). Briefly, the instrument collected ambient aerosol particles on a quartz-fiber filter for 45 min at a flow rate of 8 L min^{-1} and then analyzed them by the thermal-optical-transmittance (TOT) method for 15 min. The measurement procedure of the EC/OC analyzer used in this study is given in

Miyazaki et al. [2006]. The NO_x mixing ratios were measured using a NO_x analyzer (Thermo Scientific, Waltham, MA). The instrument collected ambient $PM_{1.0}$ particles on a quartz-fiber filter for 45 min at a flow rate of 8 L min^{-1}. The collected particles were then analyzed using the thermal-optical-transmittance (TOT) method for 15 min. Using the measured mass concentrations of OC and WSOC, water-insoluble OC (WIOC) is defined as WIOC = OC − WSOC. In the present study, the mass concentrations of WSOC and WIOC were converted to water-soluble organic matter (WSOM) and water-insoluble organic matter (WIOM). A factor of 1.8 was used for the conversion of WSOC to WSOM [*Yttri et al*., 2007; *Finessi et al*., 2012], and a factor of 1.2 was used to convert the mass of WIOC to that of WIOM [*Wang et al*., 2005].

The inorganic bulk composition of aerosols was also obtained using another PILS coupled to two ion chromatographs (IC) (761 Compact IC, Metrohm Switzerland) [*Orsini et al*., 2003] with another inlet including a $PM_{1.0}$ cyclone. The mass concentrations of sulfate (SO_4^{2-}) and other inorganic components were obtained every 15 min. The mass contributions of inorganics other than sulfate to the submicron particle mass were insignificant: the average mass concentrations of nitrate and ammonium were less than 15% of that of sulfate. Consequently, the fractions of those inorganic components are not shown in this study. PILS-IC data were obtained during a limited period (9:00–23:00 LT on 7 July; 0:00–14:00 LT on 12 July; 10:00 LT on 13 July to 22:00LT on 15 July) due to a problem with the instrument. The inorganic compositions were also measured with a filter-based off-line method as described below.

A high-volume Andersen sampler was used to collect $PM_{1.0}$ samples on quartz filters at a flow rate of 670 L min^{-1}. The sampling duration was ~3 h during the day and ~6 h at night. Only during the period from 5 to 8 July, the filter sample was obtained every 12 h. Inorganic ions were measured using the same type of IC as used for the PILS measurement during the period of 4 to 12 July. Briefly, inorganic ions were extracted from the filter samples (20 mm diameter punch) with 10 mL of ultrapure water under ultrasonication. The extracts were penetrated through a syringe filter (Millex-GV, 0.22 μm, Millipore), before being injected into the IC [*Miyazaki et al*., 2009]. Concentrations of sulfate measured with PILS-IC ($sulfate_{PILS}$) agreed with those of the filter measurement ($sulfate_{filter}$) to within 10% for the data obtained on 7 July. Although the data used for the comparison was limited, it indicates that $sulfate_{PILS}$ was almost identical to $sulfate_{filter}$ in the current study.

3. Results and Discussion

3.1. Temporal Variation

Figures 3a–3d show the temporal variations of the local wind speed and directions and the chemical composition of the observed aerosols. We observed three distinct periods in terms of different characteristics of the observed air masses. The predominant local wind directions during 4–8 July were easterly and southeasterly with typical local wind speeds $>$1.5 m s^{-1} (average 2.2 ± 0.7 m s^{-1}; Figure 3a). Consequently, the air sampled during this period was frequently influenced by emissions from urban areas (Figure 1). During the period from 8 to 11 July, the local wind speed was generally low ($<$ 1.5 m s^{-1} with an average of 1.5 ± 0.8 m s^{-1}), indicating that the observed air masses stagnated and were influenced by local emissions from the surrounding area. On the other hand, the local wind direction from 11 to 17 July was northwesterly with the average wind speed of 1.3 ± 0.8 m s^{-1}. Based on these differences in the local wind speeds and wind direction, we defined the three periods as P1, P2, and P3, respectively. GF measurements for P3 are not available.

3.1.1. Aerosol Chemical Composition

The averages values of the mass concentrations and fractions of the major chemical components for each period are summerized in Table S1 in the supporting information. During P1, sulfate (5.20 ± 3.65 μg m^{-3}) was the most abundant accounting for 62.0% of the submicron particle mass measured during that period. On 6 July (P1), the sulfate concentration showed a substantial increase with a maximum of 11.42 μg m^{-3} (Figure 3b). Conversely, the mass concentrations and fractions of organics during P2 and P3 were much larger than those during P1 as shown in Figures 3b–3d. The result clearly shows the change in the chemical compositions from sulfate-rich aerosols during P1 to organic-rich aerosols during P2/P3. The difference in the chemical compositions in the observed aerosol during each period can be explained by the difference in the local wind speeds and wind direction. As described above, the average local wind speed during P1 (2.2 ± 0.7 m s^{-1}) was higher than that during P2 (1.5 ± 0.8 m s^{-1}) and P3 (1.3 ± 0.8 m s^{-1}; Figure 3a). During P1, the predominant local winds were east to southeasterly, suggesting that most of the observed

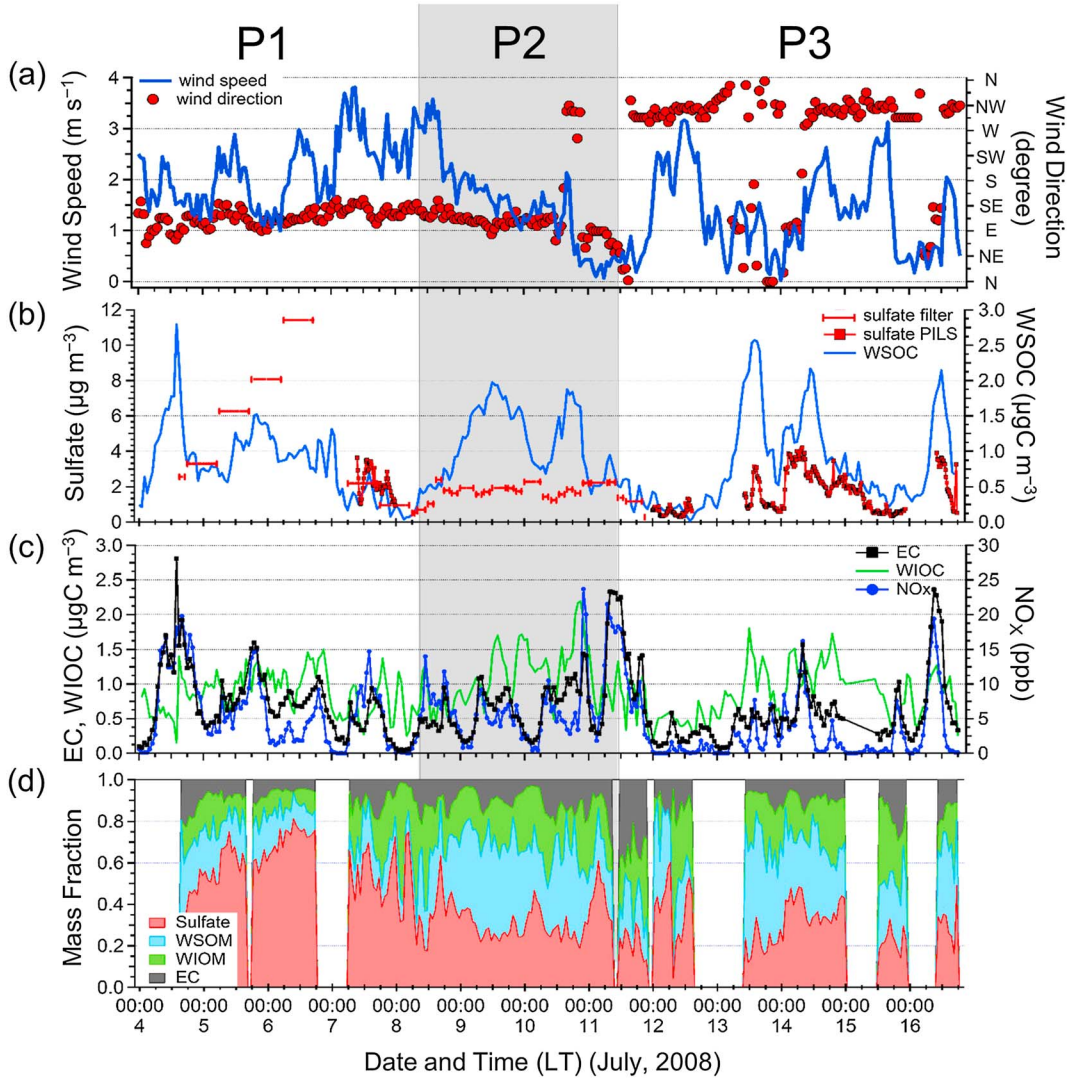

Figure 3. Time series of (a) local wind speeds and direction; (b) the concentrations of sulfate and WSOC; (c) EC, WIOC, and NO_x mixing ratios; and (d) the mass fraction of the measured component of submicron aerosols during the periods of 4–16 July 2008. Shaded area divides three periods (P1, P2, and P3).

air masses were transported from the urban industrial areas, as described in section 2.1. This explains the observed sulfate-rich aerosols, most of which were likely of anthropogenic origin. Although the predominant wind direction during P2 was similar to that during P1, the lower local wind speeds and the lower levels of sulfate during P2 suggest a difference in the dominant source of the air masses compared with P1. The predominant wind direction during P3 was northwesterly, which indicates the influence of emissions from vegetation and residential areas, as described in section 2.1. The chemical characteristics of the aerosols with the dominance of organics during P3 were rather similar to that observed during P2.

In order to investigate possible sources of organics, Figure 4 presents the WSOC and WIOC concentrations as a function of EC for each period. The average concentrations of EC were similar in each period (0.62–0.70 μg C m^{-3}; Table S1) and the temporal variations in the EC concentrations generally agreed well with those in the NO_x mixing ratios during the entire period (R^2 = 0.71, Figure 3c). In urban areas, traffic emissions have been found to be the dominant source for NO_x, whereas EC is emitted by motor vehicles with burning diesel [e.g., *Seinfeld and Pandis*, 2006]. Indeed, *Gu et al*. [2011] reported that large concentrations of EC correlate well with those of NO_x in an urban environment and they attributed the dominant source of EC to traffic emission. Therefore, our result indicates that the majority of the observed EC originated from combustion-derived sources, most likely traffic emissions. During P1 only, the WSOC showed a positive correlation with EC

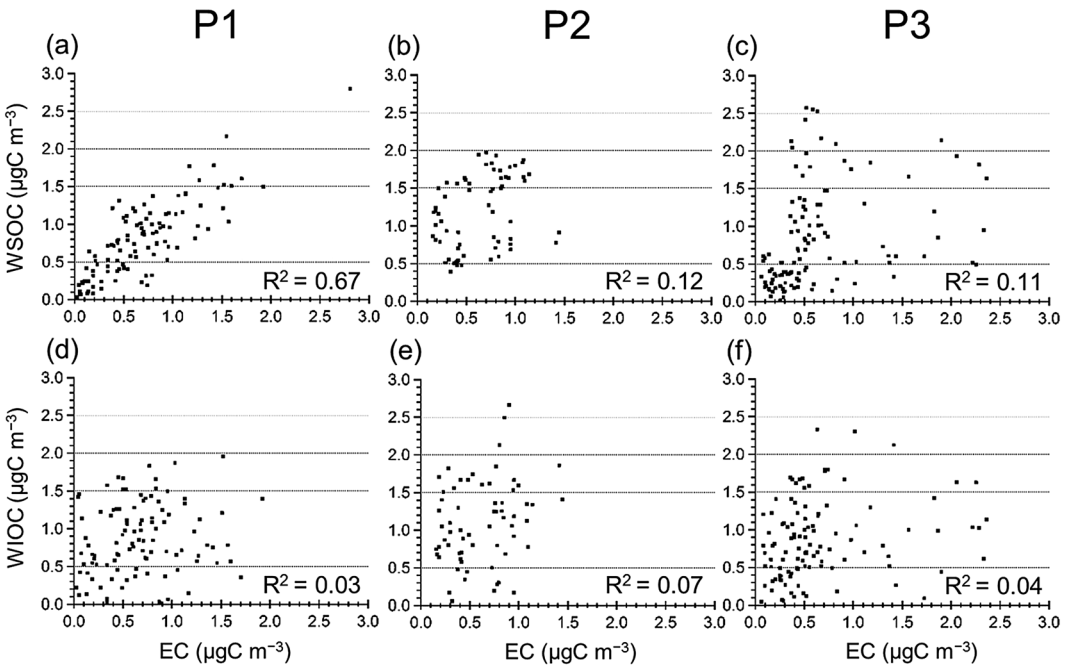

Figure 4. Scatterplots of (a–c) water-soluble organic carbon (WSOC) and (d–f) water-insoluble organic carbon (WIOC) versus elemental carbon (EC) for the periods P1, P2, and P3.

(Figure 4a), whereas the correlations were insignificant during P2 and P3 (Figures 4b and 4c). This result and the possible source of EC as discussed above suggest that combustion-derived anthropogenic sources were the dominant sources of WSOC during P1. The result of the correlation and the larger concentrations of sulfate indicate the presence of more anthropogenically influenced aerosols during P1.

In contrast, the WSOC and WIOC concentrations showed insignificant correlations with EC, with a substantial decrease in the sulfate concentrations both during P2 and P3 (Figures 4b, 4c, 4e, and 4f). This indicates that the majority of observed WSOC and WIOC during these periods did not originate from combustion-derived anthropogenic sources. Moreover, the diurnal profiles of the WSOC concentrations showed peaks during the daytime of these two periods, as shown in Figure 3b. These results suggest that the effects of local biogenic sources surrounding the study site (Figure 1) and the subsequent formation of OA on the temporal variations in WSOC were significant compared with variations due to the regional transport of air masses. In fact, *Pavuluri et al*. [2013] measured radiocarbon (^{14}C) of WSOC observed at the same sampling site in summer, which allows the quantitative apportionment between fossil fuel (dead carbon) and biogenic (modern carbon) sources. Based on this method, they found that 88% of WSOC consists of biogenic carbon, which supports the present result.

3.1.2. Number Concentrations and CCN Activity

Figures 5a and 5b show a time series of the size distribution of particle number concentrations and the N_{CN} during the study period. The N_{CN} at D_{dry} = 20.2–429 nm ranged from 230 cm^{-3} to 5440 cm^{-3}, with an average of 1560 cm^{-3}. This range is similar to that reported in previous field studies conducted at the same sampling site [*Jung et al.*, 2013; *Jung and Kawamura*, 2014]. The N_{CN} reached a maximum at the dominant size range in the Aitken mode (D_{dry} = 30–100 nm). The maximum of N_{CN} in the nucleation and Aitken modes was also reported by previous field measurements at the same sampling site [*Jung et al.*, 2013]. The measured N_{CN} in this study generally ranges from 1000 to 10,000 cm^{-3}, which is typical of rural sites [e.g., *Hussein et al.*, 2004] in northern latitudes.

In this study, a D_{dry} of 146 nm was chosen as typical size for CCN at which particles with even low hygroscopicity in the ambient atmosphere can be activated at a SS of 0.1% [*Dusek et al.*, 2006; *Petters and Kreidenweis*, 2007; *Mochida et al.*, 2010]. The N_{CCN}/N_{CN} ratio showed a wide range between 0.04 and 1.02 with an uncertainty of 10% at a SS of 0.1% (Figure 5c). It is noted that the ratio larger than 1 is physically unrealistic, which can be explained by the measurement uncertainties of the CPC and OPC for the low particle concentrations

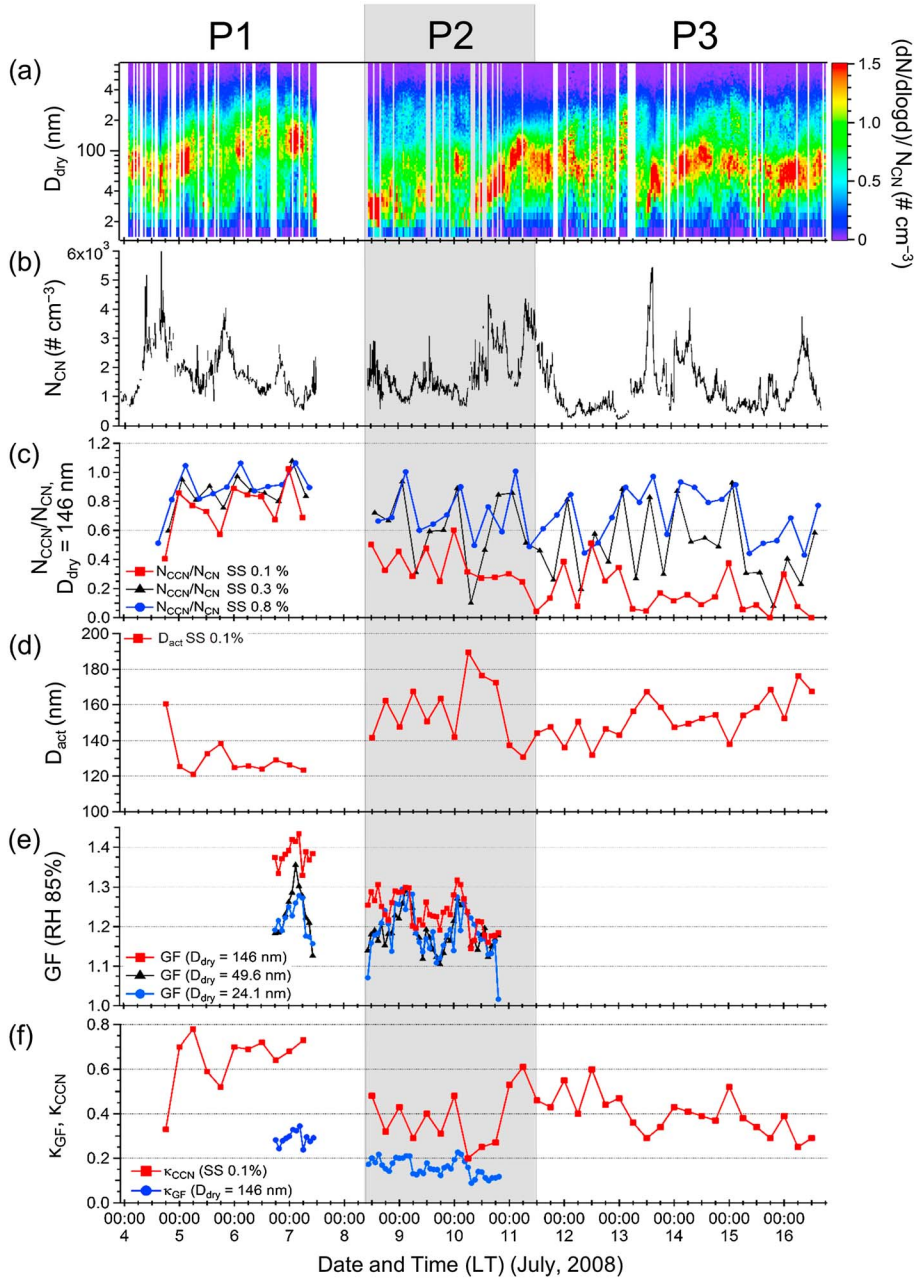

Figure 5. Time series of (a) the particle number size distribution; (b) the total particle number concentration (N_{CN}); (c) N_{CCN}/N_{CN} ratios (D_{dry} = 146 nm) at supersaturations (SS) of 0.1%, 0.3%, and 0.8%; (d) activation diameter D_{act} at SS of 0.1%; (e) hygroscopic growth factors (GF) for dry mobility sizes 146 nm, 49.6 nm, and 24.1 nm under RH of 85%; and (f) hygroscopicity parameter kappa (κ) values each obtained by the GF (D_{dry} = 146 nm) and CCN (SS = 0.1%) measurements.

at a SS of 0.1%. The wide range of the ratio indicates the presence of particles with different CCN activation properties. The N_{CCN}/N_{CN} ratios and their temporal variations were rather similar at each SS during P1, whereas the ratios at SS = 0.1% were much smaller than those at SS = 0.3% and 0.8% during P2 and P3 (Figure 5c). The similarity in the N_{CCN}/N_{CN} ratios with larger values during P1 suggests that the particles were highly CCN active, which did not significantly depend on SS, indicating internally mixed particles with highly hygroscopic chemical composition. This is supported by the dominance of sulfate during P1 (Figure 3d). On the other hand, the larger difference in the N_{CCN}/N_{CN} ratio at a different SS suggests that the majority of the observed particles during P2 and P3, even if they were in the same aerosol population, was externally mixed with different CCN characteristics. Similar results were obtained by *Silvergren et al.* [2014]

who found that the N_{CCN}/N_{CN} ratio was less sensitive to SS for highly hygroscopic, internally mixed particles, whereas the sensitivity was high for less hygroscopic, externally mixed particles influenced by anthropogenic emissions. In summary, the difference in the N_{CCN}/N_{CN} ratios among the different SS values in this study indicates that the reduction of the CCN activity depends on the chemical composition and mixing state of the observed aerosols.

Figure 5d presents temporal variations of activation diameter D_{act} at a SS of 0.1%. The average values at SS of 0.1%, 0.3%, and 0.8% during each period are shown in Table S2. The average D_{act} values during P2 and P3 were 156.8 ± 17.1 nm and 152.4 ± 11.0 nm, respectively, which are substantially larger than that during P1 (130.1 ± 10.7 nm). These D_{act} values correspond to the average κ_{CCN} values of 0.64 ± 0.12, 0.38 ± 0.12, and 0.40 ± 0.09 for P1, P2, and P3, respectively (Table S2). The differences in D_{act} and κ_{CCN} during each period suggest that the CCN were less active during P2 and P3 than during P1.

New particle formation (NPF) for particles with $D_{dry} < 30$ nm and subsequent growth of the particles were observed on 9–11 July during P2 (Figure 5a). Several NPF events in summer were also reported for the same site in our previous studies [e.g., *Jung et al.*, 2013]. An increase in the number concentrations of the particles with D_{dry} = 146 nm was observed, whereas the N_{CCN}/N_{CN} ratios at a SS of 0.1% decreased. This suggests that NPF and subsequent growth of the particles resulted in the increased number concentrations of less CCN-active particles. Note that a significant decrease of the N_{CCN}/N_{CN} ratios at a SS of 0.1% was observed during P2/P3 rather than during P1 (Figure 5c), in spite of the similarity in the number size distribution (Figure 5a). The suppression of the CCN activity during P2 and P3 can therefore be related to the change in the chemical composition and mixing state of the particles.

3.1.3. Hygroscopic Growth Factor

Figure 5e shows the temporal variation of the GF for particles at each measured diameter, whereas the average values during each period are summarized in Table S3. Although the hygroscopic GF data were obtained during the limited period of P1 and P2, a significant difference in the GF values was observed between these two periods. The average GF at D_{dry} = 146 nm during P1 (1.37 ± 0.04) was larger than those during P2 (1.24 ± 0.05). The observed GF values in the current study generally agree with those (1.19–1.27) at D_{dry} of 120 nm, obtained at the same site in summer 2011 [*Jung and Kawamura*, 2014]. Other studies reported GF values of 1.20–1.50 at similar values of D_{dry} at a suburban site in Paris [*Jurányi et al.*, 2013; *Laborde et al.*, 2013]. The larger GF values were associated with aged air masses in those previous studies, similar to those observed during P1 in this study.

Table 1 lists typical GF values for different types of aerosols reported in previous studies. *Shingler et al*. [2016] reported that the GF differs as a function of air mass origin (e.g., wildfires, agricultural fires, biogenic, marine, and urban outflow), based on the aircraft measurement conducted mainly over the United States. In this study, the observed GF of 1.37 at D_{dry} of 146 nm, obtained during P1, is close to the lower end of GF for AS (1.50–1.70). This is consistent with the aerosol chemical measurements, which showed the dominant contribution of sulfate to the submicron particle mass as discussed above. In contrast, the GF for the smaller particles ($D_{dry} < 50$ nm) in P2 (1.19; Table S3) is rather similar to typical values for secondary organic aerosols (SOA; 1.03–1.16) [*Virkkula et al.*, 1999; *Saathoff et al.*, 2003; *Varutbangkul et al.*, 2006; *Duplissy et al.*, 2011] and EC (< 1.05) [*Weingartner et al.*, 1997] (Table 1). The enrichment of sulfate in the accumulation mode, and the largest fraction of organic mass being found in the Aitken size mode, has also been found in other environments [*Pöschl et al.*, 2010; *Whitehead et al.*, 2016]. Our data suggest that the GF depends on the particle size, which is attributable to the size-dependent chemical composition. This point is further discussed in section 3.3.

In order to discuss the link between hygroscopicity at each particle size and chemical composition, Figures 6a–6c show temporal variations in the particle number concentrations as a function of the GF at D_{dry} of 146 nm, 49.6 nm, and 24.1 nm. The GF and particle number distributions indicate a large dependence of the GF on the particle size. The GF at D_{dry} = 146 nm during P1 showed a unimodal distribution with a peak as high as 1.40, which is more significant than those at smaller particle sizes (49.6 and 24.1 nm as seen in Figures 6b and 6c, respectively). This result supports the idea that most of the particles were internally mixed during P1, with the dominance of sulfate mostly residing in the accumulation size mode, as discussed above. For the smaller particles (D_{dry} = 24.1 and 49.6 nm), bimodal GF distributions became more pronounced during P2, which supports the idea that the majority of the particles were externally mixed during this period. The contributions of the particle number to the high GF values were more significant at these smaller sizes

Table 1. Typical Values of Hygroscopic Growth Factor (GF) for Various Aerosol Components Reported in Previous Studies

Composition/Source of Aerosol	Growth Factor (GF)	RH	Reference
BC, mineral dust	< 1.05	94%, 95%	*Weingartner et al.* [1997] and *Vlasenko et al.* [2005]
Biomass burning	1.15–1.65 (GF differs depending on the mixing state with secondary inorganic ions)	75–95%	*Cocker et al.* [2001], *Shingler et al.* [2016], and *Swietlicki et al.* [2008]
Ammonium sulfate $(NH_4)_2SO_4$, ammonium nitrate NH_4NO_3	1.5–1.7	85%, 90%	*Gysel et al.* [2002], *Wise et al.* [2003], and Swietlicki et al. [2008]
Urban	1.20–1.43	75–95%	*Shingler et al.* [2016]
Secondary organic aerosol (SOA)	1.01–1.16 (up to 1.65 for aged SOA in a simulation chamber)	84–95%	*Virkkula et al.* [1999], *Saathoff et al.* [2003], *Varutbangkul et al.* [2006], and *Duplissy et al.* [2011]
Biogenic	1.20–1.45	75–95%	*Shingler et al.* [2016]
Organic compounds (e.g., oxalic acid, malonic acid, fulvic acid, levoglucosan)	1.0–1.7	80–95%	*Peng et al.* [2001], *Chan and Chan* [2003], *Prenni et al.* [2001], *Wise et al.* [2003], *Huff Hartz et al.* [2006], and *Koehler et al.* [2006]
Secondary organic aerosols from terpenes, α-pinene, β-pinene	1.03–1.18	85%, 90%	*Saathoff et al.* [2003], *Varutbangkul et al.* [2006], and *Prenni et al.* [2007]
Sea-salt, sulfuric acid	> 2.0	90%, 95%	*Gysel et al.* [2002] and *Koehler et al.* [2006]
Marine	1.35–1.60	75–95%	*Shingler et al.* [2016]

(Figures 6b and 6c). This is attributable to the increase in the particle number concentrations in the Aitken mode (Figures 5a and 5b) with less aged characteristics of the particles of local origin.

3.2. Supersaturated and Subsaturated Hygroscopicity

Figure 5f shows the temporal variations of the κ_{CCN} and κ_{GF}. Overall, the average κ_{CCN} (0.24 ± 0.16) observed in this study is similar to those reported for a suburban site in Paris (κ_{CCN} = 0.08–0.24 at SS of 0.1–1.0%)

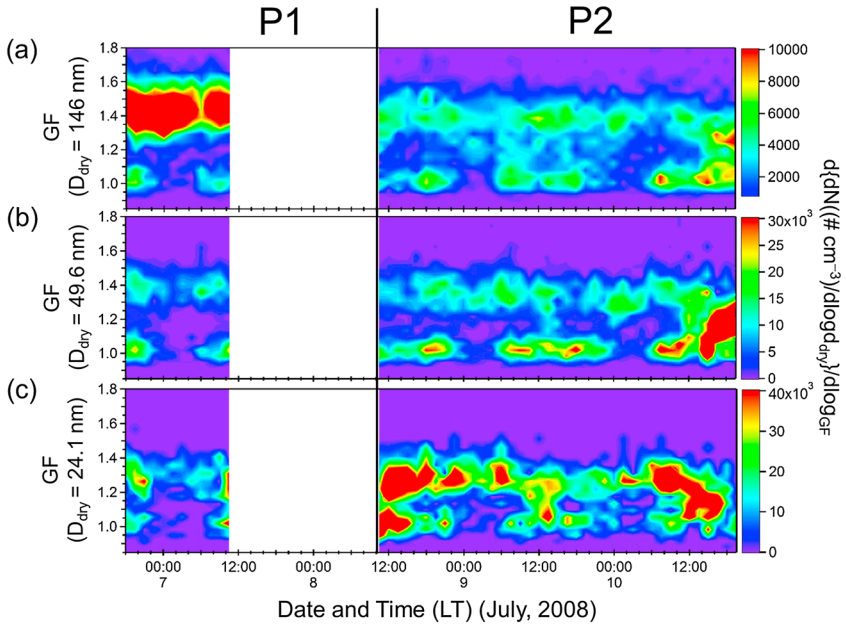

Figure 6. Temporal variations in the particle number concentrations as a function of the growth factor (GF) at D_{dry} of (a) 146 nm, (b) 49.6 nm, and (c) 24.1 nm.

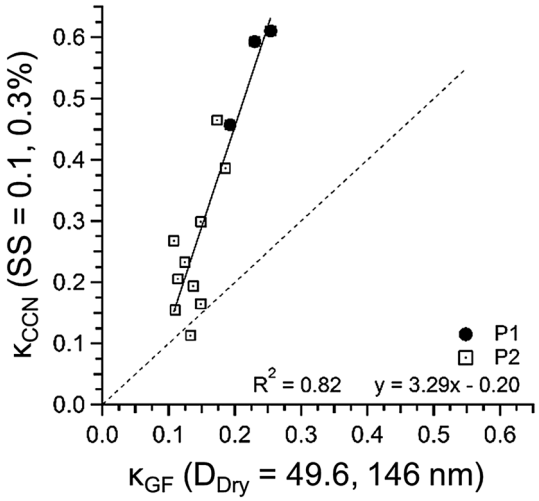

Figure 7. Scatterplot of κ_{CCN} versus κ_{GF}. The average κ_{GF} at D_{dry} of 49 and 146 nm are compared with the average κ_{CCN} at similar D_{act} under SS of 0.1% and 0.3%. The data obtained during P1 and P2 are indicated by solid circles and open squares, respectively.

[*Jurányi et al.*, 2013]. As expected from the GF values, the κ_{CCN} and κ_{GF} during P1 were significantly larger than those during P2 and P3 (also summarized in Table S4), exhibiting greater hygroscopicity during P1 under both supersaturated and subsaturated conditions. In order to examine the κ values derived from the CCNC and HTDMA measurements, Figure 7 compares the average κ_{GF} (D_{dry} = 49, 146 nm) with κ_{CCN} values at similar D_{act} ranges (47.34–129.04 nm for P1; 69.81–189.54 nm for P2) obtained at SS of 0.1 and 0.3%. While the κ_{CCN} under all SS conditions correlated well with the corresponding κ_{GF} (R^2 = 0.82), the κ_{CCN} was generally larger than the κ_{GF} by 59% and 44% for P1 and P2, respectively. The degree of the difference in our study is similar to that (~37%) found for ambient aerosols at a mountainous site in central Germany [*Wu et al.*, 2013] and at an urban site in Japan [*Kawana et al.*, 2016].

Discrepancies between CCNC-derived and HTDMA-derived κ values have been reported in a number of previous studies, which have generally reported larger κ_{CCN} compared to κ_{GF} [*Roberts et al.*, 2010; *Cerully et al.*, 2011; *Hersey et al.*, 2013; *Hong et al.*, 2014; *Hansen et al.*, 2015]. Although *Carrico et al.* [2008] reported that κ_{CCN} and κ_{GF} (at RH = 90%) for laboratory-generated biomass burning particles agreed to within 20% and *Dusek et al.* [2011] also showed the agreement between κ_{CCN} and κ_{GF} (at RH = 85%) for particles with diameters of 100–150 nm, the difference between them increased with decreasing particles size. *Irwin et al.* [2010] found that the discrepancy between κ_{CCN} and κ_{GF} (at RH = 86%) increased with decreasing particle size for particles measured at a mountainous site in Germany. These discrepancies can be attributed to several factors: the differences in the size dependence of chemical compositions, the effects of solutes on water activity under subsaturated and supersaturated conditions particularly in the presence of organic compounds, and particle mixing state [*Roberts et al.*, 2010; *Hersey et al.*, 2013; *Hong et al.*, 2014]. In general, surface active organic compounds decrease the surface tension of particles and reduce the surface tension effect (Kelvin effect) [*Wex et al.*, 2008], which increases CCN activity [*Sorjamaa et al.*, 2004; *Wex et al.*, 2008; *Irwin et al.*, 2010; *Dusek et al.*, 2011]. The effect of the surface tension becomes more important for particles in the smaller size range (e.g., <~170 nm), because a certain amount of surfactant is more concentrated in a droplet of solution formed on smaller particles rather than larger ones [*Sorjamaa et al.*, 2004; *Wex et al.*, 2008; *Irwin et al.*, 2010; *Dusek et al.*, 2011]. On the other hand, the partitioning from bulk to surface of a particle decreases the concentration of the bulk solute with increasing the fraction of surfactants. This increases the water activity (Raoult effect) of the droplet and can compensate the reduction of the surface tension at the droplet-air interface, which reduces CCN activity [*Li et al.*, 1998; *Rood and Williams*, 2001; *Sorjamaa et al.*, 2004; *Wex et al.*, 2008; *Frosch et al.*, 2011; *Renbaum-Wolff et al.*, 2016]. Therefore, changes in the surface tension and the presence of organics can largely affect the particle hygroscopicity under supersaturated condition. In contrast, hygroscopic growth under subsaturated condition is insensitive toward changes in the surface tension [*Wex et al.*, 2008]. Consequently, the above effects can contribute to the discrepancy between κ_{CCN} and κ_{GF}.

With regard to the effect of the mixing state, for example, *Hersey et al.* [2013] suggested that a transition from externally mixed to internally mixed aerosols, as the aerosols evolved from west to east of the Los Angeles Basin, leads to an increased difference between κ_{CCN} and κ_{GF}. Photochemical aging of particles results in the conversion of externally mixed to internally mixed particles, which enhanced κ_{CCN} with increasing coating thickness on refractory black carbon in their case. In contrast, the aging resulted in the suppressed subsaturated water uptake (κ_{GF}) of the main hygroscopic mode, which is attributable to the formation of

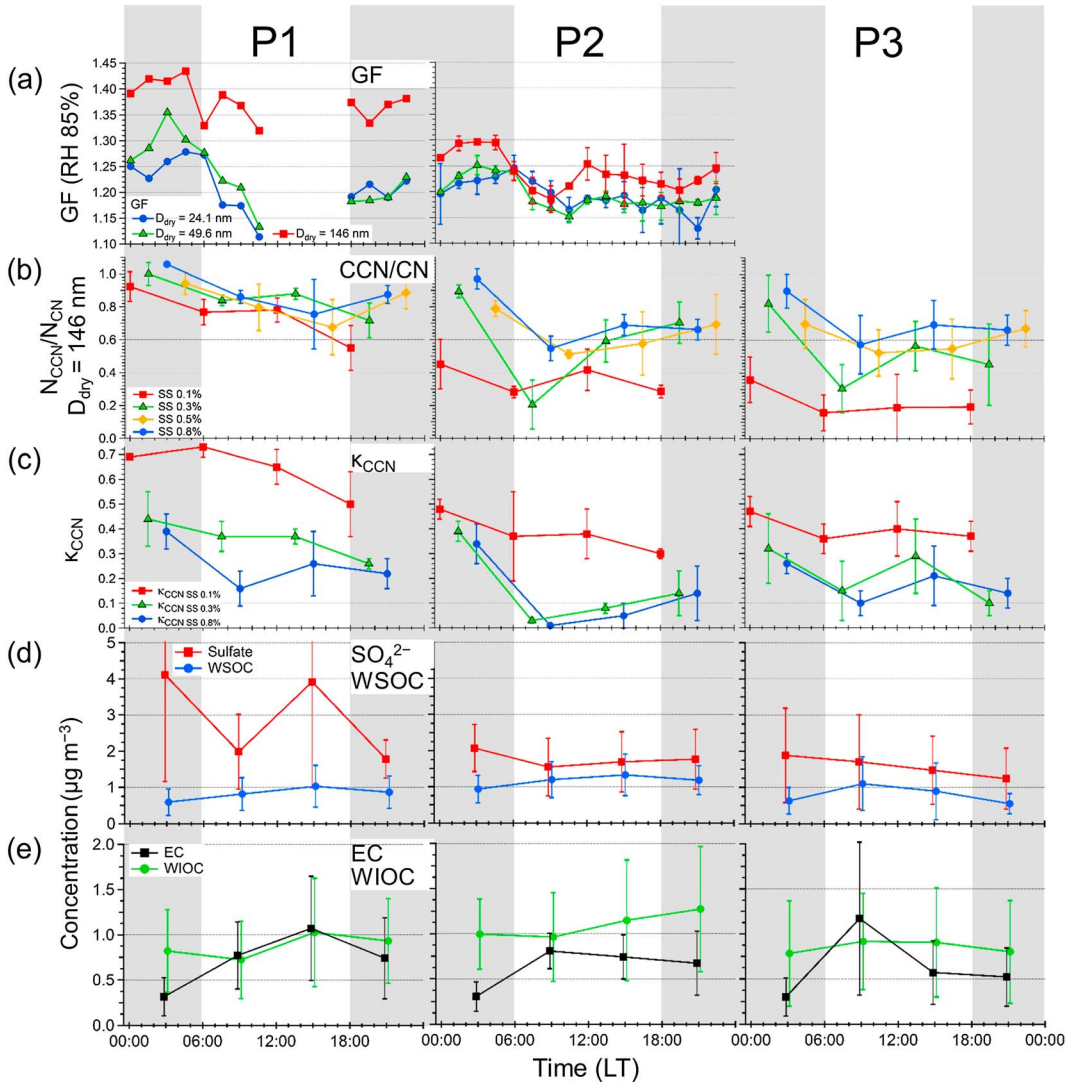

Figure 8. Diurnal profiles of (a) growth factors (GF) at RH of 85%; (b) N_{CCN}/N_{CN} ratios for particles with dry mobility diameter of 146 nm; (c) κ_{CCN} under SS of 0.1%, 0.3%, and 0.8%; the mass concentrations of (d) sulfate and water-soluble organic carbon (WSOC); and (e) water-insoluble organic carbon (WIOC) and elemental carbon (EC). Bars indicate $\pm 1\sigma$ (standard deviation) of each average value. Shaded area indicates the nighttime.

separate, organic layers that inhibit the water uptake during humidification under the conditions of the κ_{GF} measurement. These effects can also explain the increased discrepancy between κ_{GF} and κ_{CCN} for aged aerosols. In this study, the reduced difference between κ_{CCN} and κ_{GF} during P2 (Figure 5f) indicates the dominance of externally mixed aerosols compared with the sulfate-rich, internally mixed aged aerosols observed during P1. Indeed, the GF distributions presented in Figures 6a–6c demonstrate that the observed particles show bimodal distributions during P2 and thus are indicative of the external mixture. On the other hand, the unimodal GF distribution during P1 supports the idea that most of the particles were internally mixed during this period.

3.3. Diurnal Variations and Size Dependence of Particle Hygroscopicity

Figure 8 shows diurnal profiles of the GF, N_{CCN}/N_{CN} ratio, and κ_{CCN}, in relation to the chemical compositions for each period. The bulk GF values at night (1.30 ± 0.08 for P1 and 1.24 ± 0.05 for P2) were larger than those in the daytime (1.24 ± 0.09 for P1 and 1.18 ± 0.03 for P2). A similar difference was also observed for κ_{CCN}, particularly during P2, when the κ_{CCN} in the daytime (0.14 ± 0.14) was substantially lower than that (0.31 ± 0.13) at night (Table S4). The larger hygroscopicity at 0:00–6:00 LT can be attributed to the increased

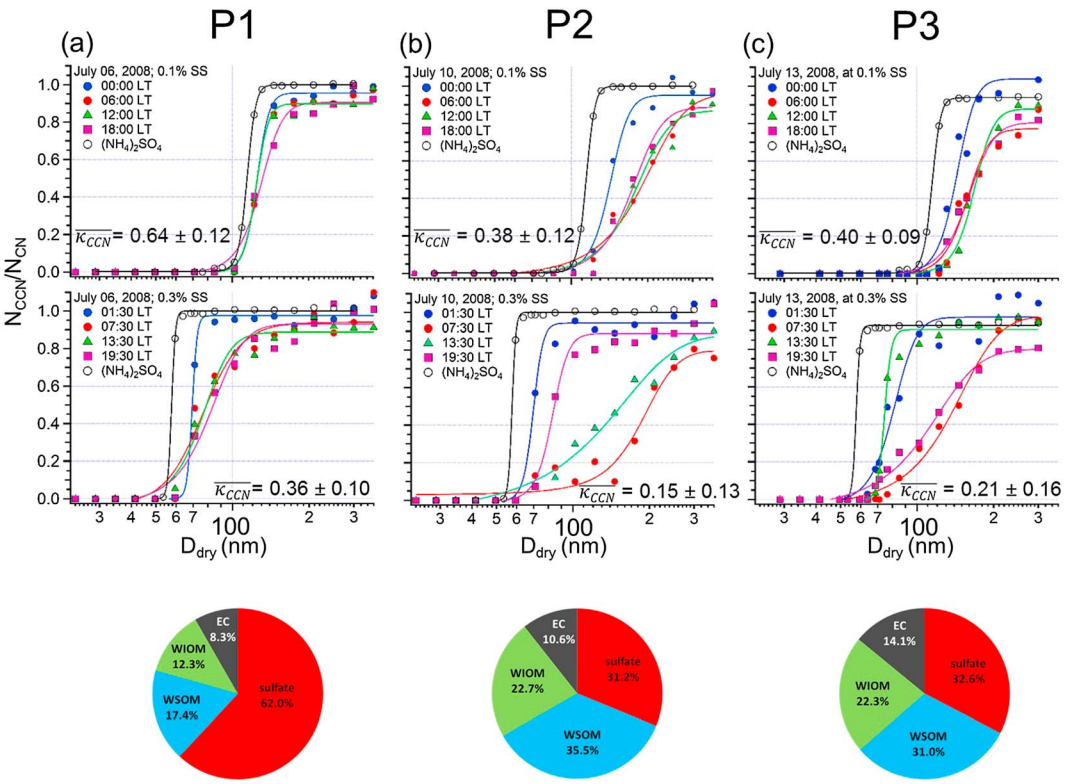

Figure 9. Diurnal changes in the N_{CCN}/N_{CN} efficiency spectra at SS of 0.1% and 0.3% on (a) 6, (b) 10, and (c) 13 July 2008, as representatives of periods P1, P2, and P3, respectively. The efficiency spectra was fitted usung a cumulative distribution function given by *Rose et al.* [2008]. Pie chart shows the mass fractions of sulfate, WSOM, WIOM, and EC during each period.

concentrations of sulfate. Figure 9 displays diurnal changes of the N_{CCN}/N_{CN} efficiency spectra as a function of D_{dry} at a SS of 0.1% and 0.3%, as representative profiles during each period. Indeed, the typical CCN spectra during the nighttime of P1 were similar to that of AS (Figure 9a), which is consistent with the chemical measurements exhibiting substantial mass fractions of sulfate (62.0 ± 43.5%) in the submicron particles. Even during P2, the CCN spectra at 00:00–01:30 were similar to those of AS (Figure 9b). This result supports the idea that the greater hygroscopicity at 0:00–6:00 LT can be attributed to the increased concentrations and mass fractions of sulfate.

Particles with $D_{dry} < 100$ nm for 0.3% SS during P1 activated more readily than those during P2 and P3 (Figure 9). The CCN efficiency curves exhibit a much larger difference in the D_{act} between the ambient and AS particles during the daytime of P2 and P3. In general, the broad sigmoid of the CCN spectra is closely related to the heterogeneity of the aerosol chemical composition [*Moore et al.*, 2010; *Padró et al.*, 2012]. Combined with the bimodal GF distribution during the daytime of P2 (Figure 6), the result indicates a larger degree of external mixture during these periods. This is particularly true for the particles at 0.3% SS, which emphasizes the increase of less-CCN active particles during the daytime. This can be explained by the increased concentrations of organics and EC during the day in P2 and P3 as shown in Figures 8d and 8e. These observations indicate that increased organics and EC concentrations suppressed the particle hygroscopicity during the day. The hygroscopicity of particles that activated at SS = 0.1% in the accumulation mode (Figure 9) is probably less affected by the diurnal changes in those emissions. This indicates that the suppression of κ_{CCN} in the smaller size ranges was attributable to these organics and EC. Similarly, *Crosbie et al.* [2015] reported that the lowest hygroscopicity values correspond with the maximum concentrations of EC and OC, which they found in the early morning in Central Tucson. On the other hand, during nighttime, internally mixed aerosols dominated by sulfate increased the hygroscopicity of particles during P1 in this study (Figure 8c).

Many of the previous studies showed diurnal cycles of particle hygroscopicity, with peaks typically appearing in the afternoon in urban [*Crosbie et al.*, 2015], rural [*Cerully et al.*, 2015], marine [*Kalivitis et al.*, 2015], boreal forest, and grassland areas [*Paramonov et al.*, 2015]. This has been explained by atmospheric aging of

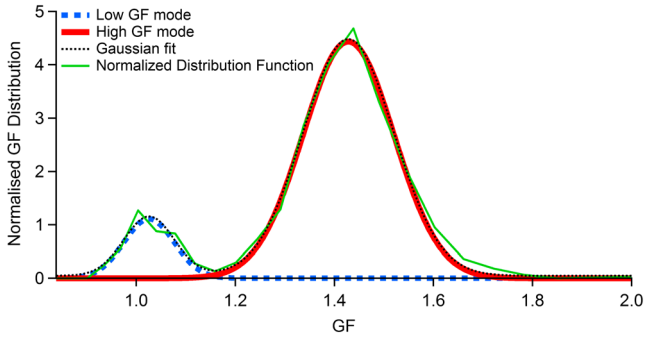

Figure 10. Example of a bimodal GF distribution. For the definition of high GF (N_{HGF}) and low GF (N_{LGF}) modes, see text. The GF distribution are calculated using a multiple Gaussian fit applied on the normalized distribution function. Separation of the modes was made by cluster analysis using the program IGOR Pro.

aerosols through condensational growth of photochemically oxidized organics and sulfate. The diurnal pattern obtained in this study is rather similar to those reported for observational sites at higher altitudes in France, and in the central Himalayas [*Holmgren et al.*, 2014; *Dumka et al.*, 2015]. *Holmgren et al.* [2014] and *Dumka et al.* [2015] attributed the lower hygroscopicity during the daytime to the reduced influence of anthropogenic emissions on the observed aerosols due to the lifting of the planetary boundary layer.

To further investigate the GF mode, we derived a distribution function for each GF obtained every 90 min for each particle size (D_{dry} = 24.1 nm, 49.6 nm, and 146 nm) between 6 and 10 July. Figure 10 presents a typical example of the observed bimodal GF distribution function for the particle size of 146 nm, measured during a specific time period (18:00–19:30) on 6 July. The figure shows two peaks in the GF distribution, where one peak was observed at the GF of ~1.02 and the other one at the GF of ~1.40. The particle number fractions of low and high GF modes are defined as N_{LGF} and N_{HGF}, respectively. The peaks for each size-segregated bimodal GF distribution are calculated using a multiple Gaussian fit. As introduced in section 2.3, cluster analysis is applied to calculate the fraction of the particle number concentration of low and high GF modes; the peaks of the low and high GF modes were 1.02 and 1.35, respectively. Figure 11a shows the temporal variations of N_{LGF} and N_{HGF}, for particles at D_{dry} = 49.6 nm, whereas the N_{LGF} and N_{HGF} for particles at D_{dry} = 24.1 nm and 146 nm are shown in Figure S1. The temporal variation of N_{LGF} at D_{dry} = 49.6 nm followed that of the EC concentrations (Figure 11b). Although size-segregated EC data in the submicron range were not available in this study, the similar temporal trend indicates that the variation of the low GF in the small size particles is generally attributable to the contribution of EC.

Figure 12 shows the hygroscopic GF as a function of the WSOM-to-sulfate ratio at each D_{dry}. The hygroscopic GF values at D_{dry} = 146 nm tend to increase with decreasing WSOM-to-sulfate ratios (Figure 12a), suggesting that the hygroscopicity in the accumulation size mode depends on the abundance of OM relative to sulfate. This can explain the fact that the GF of smaller size particles does not depend on the WSOM/sulfate ratios (Figures 12b and 12c). Overall, the above result suggests that the particle hygroscopicity was suppressed

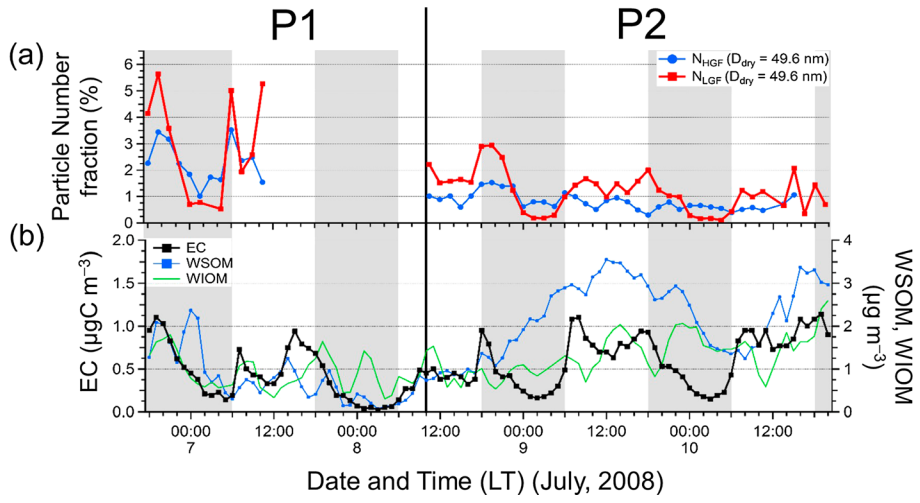

Figure 11. Temporal variations in (a) the particle number fraction for high GF mode (N_{HGF}) and low GF mode (N_{LGF}) particles at D_{dry} = 49.6 nm, and (b) the mass concentrations of EC, WSOM, and WIOM.

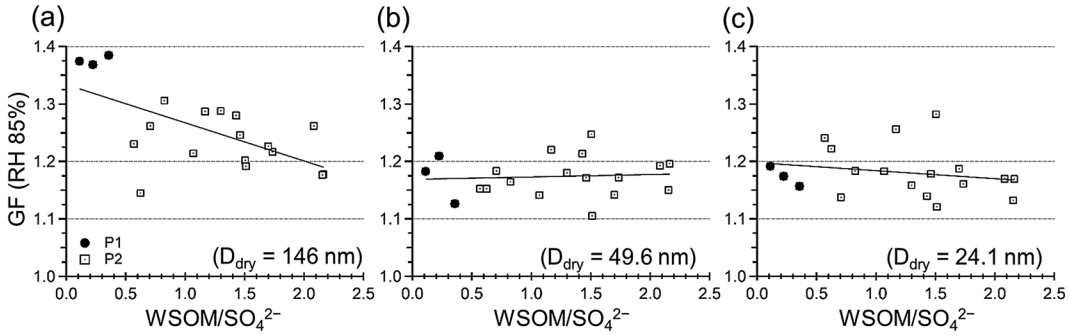

Figure 12. Scatterplot of hygroscopic GF versus ratio of the WSOM to sulfate at D_{dry} of (a) 146 nm, (b) 49.6 nm, and (c) 24.1 nm. Data during P1 and P2 are indicated by solid circles and open squares, respectively.

during P2 due to increased external mixture of less aged particles containing organics, possibly from biogenic origins, and EC. In summary, the present study shows that the more-aged internally mixed aerosol particles during P1 are of anthropogenic origin and that their higher hygroscopic properties are due to the larger fraction of sulfate. On the other hand, less aged, externally mixed, less hygroscopic particles during P2 and P3 are dominated by organic carbon of local biogenic origin. The results suggest that the abundance of OM relative to sulfate in the accumulation mode and the absolute abundance of EC in the Aitken mode are important factors controlling the hygroscopicity of submicron particles. This might be important for predicting cloud properties under similar atmospheric conditions.

4. Conclusions

Continuous in situ measurements of size-segregated CCN spectra at four supersaturations (0.1%, 0.3%, 0.5%, and 0.8%), and hygroscopic GF at 85% RH, were simultaneously conducted at a suburban site in northern Japan, in July 2008. Two distinct periods were observed in terms of differences in GF, D_{act}, and chemical compositions. The κ values derived from the CCN measurements were generally larger than those derived from the HTDMA measurements by 42–56%. The GF (1.37 ± 0.04) with D_{dry} of 146 nm and bulk N_{CCN}/N_{CN} ratios (0.83 ± 0.12) showed higher values during the first period (P1). The data suggest the dominance of internally mixed sulfate aerosols in the accumulation size mode with relatively aged characterisitics.

On the other hand, the particles observed during the latter period (P2 and P3) showed external mixing dominated by organics, which was linked to low hygroscopicity and CCN activity. In particular, higher loading of WSOM, which accounted for ~60% of OM by mass, and increased WSOM/sulfate ratios, corresponded to low GF and N_{CCN}/N_{CN} ratios with larger D_{act} in the accumulation size range. This result suggests that WSOM, probably dominated by the influence of biogenic sources, is responsible for suppressing hygroscopicity and CCN activation in the accumulation size modes in our study.

Temporal variations in the number concentrations of low GF mode at D_{dry} = 49.6 nm were similar to those in the EC concentrations, suggesting that EC contributed to the reduction of the hygroscopicity in this smaller size range. These results suggest that the abundance of OM relative to sulfate in the accumulation mode and the absolute abundance of EC in the Aitken mode are important factors controlling hygroscopicity of submicron particles. Our results demonstrate that chemical composition and particle mixing state are important factors to control hygroscopicity and CCN activation of the different size modes in the submicron particles during the study period. These results provide useful data sets of size-resolved subsaturated and supersaturated hygroscopicity for accurately predicting cloud forming potential of particles. This study also highlights the importance of the abundance of OM relative to sulfate in predicting cloud properties and their resultant climate effects in the future.

Acknowledgments
This research was supported by Grant-in-Aid for Scientific Research (19204055 and 19710004) from the Ministry of Education, Culture, Sports, Science and Technology (MEXT), Japan. We thank S. Kundu, P. Fu, G. Wang, K. Torii, S. Agarwal, S. Yamamoto, K. Matsumoto, M. Lazaar, and K. Okuzawa for their help with the aerosol sampling and M. Mochida for his help in the design and assemblage of a HTDMA system. All data used in this study are provided in the supporting information.

References

Aggarwal, S. G., M. Mochida, Y. Kitamori, and K. Kawamura (2007), Chemical closure study on hygroscopic properties of urban aerosol particles in Sapporo, Japan, *Environ. Sci. Technol.*, *41*(20), 6920–6925, doi:10.1021/es063092m.

Boreddy, S. K. R., K. Kawamura, and J. Jung (2014), Hygroscopic properties of particles nebulized from water extracts of aerosols collected at Chichijima Island in the western North Pacific: An outflow region of Asian dust, *J. Geophys. Res. Atmos.*, *119*, 167–178, doi:10.1002/2013JD020626.

Burkart, J., G. Steiner, G. Reischl, and R. Hitzenberger (2011), Long-term study of cloud condensation nuclei (CCN) activation of the atmospheric aerosol in Vienna, *Atmos. Environ.*, *45*(32), 5751–5759, doi:10.1016/j.atmosenv.2011.07.022.

Carrico, C. M., M. D. Petters, S. M. Kreidenweis, J. L. Collett Jr., G. Engling, and W. C. Malm (2008), Aerosol hygroscopicity and cloud droplet activation of extracts of filters from biomass burning experiments, *J. Geophys. Res.*, *113*, D08206, doi:10.1029/2007JD009274.

Cerully, K. M., et al. (2011), Aerosol hygroscopicity and CCN activation kinetics in a boreal forest environment during the 2007 EUCAARI campaign, *Atmos. Chem. Phys.*, *11*(23), 12,369–12,386, doi:10.5194/acp-11-12369-2011.

Cerully, K. M., A. Bougiatioti, J. R. Hite Jr., H. Guo, L. Xu, N. L. Ng, R. Weber, and A. Nenes (2015), On the link between hygroscopicity, volatility, and oxidation state of ambient and water-soluble aerosols in the southeastern United States, *Atmos. Chem. Phys.*, *15*(15), 8679–8694, doi:10.5194/acp-15-8679-2015.

Chan, M. N., and C. K. Chan (2003), Hygroscopic properties of two model humic-like substances and their mixtures with inorganics of atmospheric importance, *Environ. Sci. Technol.*, *37*(22), 5109–5115, doi:10.1021/es034272o.

Chan, M. N., and C. K. Chan (2005), Mass transfer effects in hygroscopic measurements of aerosol particles, *Atmos. Chem. Phys.*, *5*(10), 2703–2712, doi:10.5194/acp-5-2703-2005.

Cocker, D. R. I. I. I., N. E. Whitlock, R. C. Flagan, and J. H. Seinfeld (2001), Hygroscopic properties of Pasadena, California aerosol, *Aerosol Sci. Technol.*, *35*(2), 637–647, doi:10.1080/02786820120653.

Crosbie, E., J.-S. Youn, B. Balch, A. Wonaschütz, T. Shingler, Z. Wang, W. C. Conant, E. A. Betterton, and A. Sorooshian (2015), On the competition among aerosol number, size and composition in predicting CCN variability: A multi-annual field study in an urbanized desert, *Atmos. Chem. Phys.*, *15*(12), 6943–6958, doi:10.5194/acp-15-6943-2015.

Dumka, U. C., D. Bhattu, S. N. Tripathi, D. G. Kaskaoutis, and B. L. Madhavan (2015), Seasonal inhomogeneity in cloud precursors over Gangetic Himalayan region during GVAX campaign, *Atmos. Res.*, *155*, 158–175, doi:10.1016/j.atmosres.2014.11.022.

Duplissy, J., et al. (2009), Intercomparison study of six HTDMAs: Results and recommendations, *Atmos. Meas. Tech.*, *2*(2), 363–378, doi:10.5194/amt-2-363-2009.

Duplissy, J., et al. (2011), Relating hygroscopicity and composition of organic aerosol particulate matter, *Atmos. Chem. Phys.*, *11*(3), 1155–1165, doi:10.5194/acp-11-1155-2011.

Dusek, U., et al. (2006), Size matters more than chemistry for cloud-nucleating ability of aerosol particles, *Science*, *312*(5778), 1375–1378, doi:10.1126/science.1125261.

Dusek, U., G. P. Frank, A. Massling, K. Zeromskiene, Y. Iinuma, O. Schmid, G. Helas, T. Hennig, A. Wiedensohler, and M. O. Andreae (2011), Water uptake by biomass burning aerosol at sub- and supersaturated conditions: Closure studies and implications for the role of organics, *Atmos. Chem. Phys.*, *11*(18), 9519–9532, doi:10.5194/acp-11-9519-2011.

Engelhart, G. J., A. Asa-Awuku, A. Nenes, and S. N. Pandis (2008), CCN activity and droplet growth kinetics of fresh and aged monoterpene secondary organic aerosol, *Atmos. Chem. Phys.*, *8*(14), 3937–3949, doi:10.5194/acp-8-3937-2008.

Engelhart, G. J., R. H. Moore, A. Nenes, and S. N. Pandis (2011), Cloud condensation nuclei activity of isoprene secondary organic aerosol, *J. Geophys. Res.*, *116*, D02207, doi:10.1029/2010JD014706.

Farmer, D. K., C. D. Cappa, and S. M. Kreidenweis (2015), Atmospheric processes and their controlling influence on cloud condensation nuclei activity, *Chem. Rev.*, *115*(10), 4199–4217, doi:10.1021/cr5006292.

Finessi, E., et al. (2012), Determination of the biogenic secondary organic aerosol fraction in the boreal forest by NMR spectroscopy, *Atmos. Chem. Phys.*, *12*(2), 941–959, doi:10.5194/acp-12-941-2012.

Fors, E. O., E. Swietlicki, B. Svenningsson, A. Kristensson, G. P. Frank, and M. Sporre (2011), Hygroscopic properties of the ambient aerosol in southern Sweden—A two year study, *Atmos. Chem. Phys.*, *11*(16), 8343–8361, doi:10.5194/acp-11-8343-2011.

Frosch, M., N. L. Prisle, M. Bilde, Z. Varga, and G. Kiss (2011), Joint effect of organic acids and inorganic salts on cloud droplet activation, *Atmos. Chem. Phys.*, *11*(8), 3895–3911, doi:10.5194/acp-11-3895-2011.

Gu, J., et al. (2011), Source apportionment of ambient particles: Comparison of positive matrix factorization analysis applied to particle size distribution and chemical composition data, *Atmos. Environ.*, *45*(10), 1849–1857, doi:10.1016/j.atmosenv.2011.01.009.

Gysel, M., E. Weingartner, and U. Baltensperger (2002), Hygroscopicity of aerosol particles at low temperatures. 2. Theoretical and experimental hygroscopic properties of laboratory generated aerosols, *Environ. Sci. Technol.*, *36*(1), 63–68, doi:10.1021/es010055g.

Hansen, A. M. K., J. Hong, T. Raatikainen, K. Kristensen, A. Ylisirniö, A. Virtanen, T. Petäjä, M. Glasius, and N. L. Prisle (2015), Hygroscopic properties and cloud condensation nuclei activation of limonene-derived organosulfates and their mixtures with ammonium sulfate, *Atmos. Chem. Phys.*, *15*(24), 14,071–14,089, doi:10.5194/acp-15-14071-2015.

Hersey, S. P., et al. (2013), Composition and hygroscopicity of the Los Angeles aerosol: CalNex, *J. Geophys. Res. Atmos.*, *118*, 3016–3036, doi:10.1002/jgrd.50307.

Holmgren, H., K. Sellegri, M. Hervo, C. Rose, E. Freney, P. Villani, and P. Laj (2014), Hygroscopic properties and mixing state of aerosol measured at the high-altitude site Puy de Dôme (1465 m a.s.l.), France, *Atmos. Chem. Phys.*, *14*(18), 9537–9554, doi:10.5194/acp-14-9537-2014.

Hong, J., et al. (2014), Hygroscopicity, CCN and volatility properties of submicron atmospheric aerosol in a boreal forest environment during the summer of 2010, *Atmos. Chem. Phys.*, *14*(9), 4733–4748, doi:10.5194/acp-14-4733-2014.

Huff Hartz, K. E., J. E. Tischuk, M. N. Chan, C. K. Chan, N. M. Donahue, and S. N. Pandis (2006), Cloud condensation nuclei activation of limited solubility organic aerosol, *Atmos. Environ.*, *40*(4), 605–617, doi:10.1016/j.atmosenv.2005.09.076.

Hussein, T., A. Puustinen, P. P. Aalto, J. M. Mäkelä, K. Hämeri, and M. Kulmala (2004), Urban aerosol number size distributions, *Atmos. Chem. Phys.*, *4*(2), 391–411, doi:10.5194/acp-4-391-2004.

Intergovernmental Panel on Climate Change (2013), Climate Change 2013, The Physical Science Basis, in *Contribution of Working Group I to the Fifth Assessment Report of the Intergovernmental Panel on Climate Change*, edited by T. F. Stocker et al., 1535 pp., Cambridge Univ. Press, Cambridge, U. K., and New York, doi:10.1017/CBO9781107415324.

Irwin, M., N. Good, J. Crosier, T. W. Choularton, and G. McFiggans (2010), Reconciliation of measurements of hygroscopic growth and critical supersaturation of aerosol particles in central Germany, *Atmos. Chem. Phys.*, *10*(23), 11,737–11,752, doi:10.5194/acp-10-11737-2010.

Jung, J., and K. Kawamura (2014), Hygroscopic properties of newly formed ultrafine particles at an urban site surrounded by deciduous forest (Sapporo, northern Japan) during the summer of 2011, *Atmos. Chem. Phys.*, *14*(14), 7519–7531, doi:10.5194/acp-14-7519-2014.

Jung, J., Y. J. Kim, S. G. Aggarwal, and K. Kawamura (2011), Hygroscopic property of water-soluble organic-enriched aerosols in Ulaanbaatar, Mongolia during the cold winter of 2007, *Atmos. Environ.*, *45*(16), 2722–2729, doi:10.1016/j.atmosenv.2011.02.055.

Jung, J., Y. Miyazaki, and K. Kawamura (2013), Different characteristics of new particle formation between urban and deciduous forest sites in Northern Japan during the summers of 2010–2011, *Atmos. Chem. Phys.*, *13*(1), 51–68, doi:10.5194/acp-13-51-2013.

Jurányi, Z., M. Gysel, E. Weingartner, N. Bukowiecki, L. Kammermann, and U. Baltensperger (2011), A 17 month climatology of the cloud condensation nuclei number concentration at the high alpine site Jungfraujoch, *J. Geophys. Res.*, *116*, D10204, doi:10.1029/2010JD015199.

Jurányi, Z., T. Tritscher, M. Gysel, M. Laborde, L. Gomes, G. Roberts, U. Baltensperger, and E. Weingartner (2013), Hygroscopic mixing state of urban aerosol derived from size-resolved cloud condensation nuclei measurements during the MEGAPOLI campaign in Paris, *Atmos. Chem. Phys.*, *13*(13), 6431–6446, doi:10.5194/acp-13-6431-2013.

Kalivitis, N., V.-M. Kerminen, G. Kouvarakis, I. Stavroulas, A. Bougiatioti, A. Nenes, H. E. Manninen, T. Petäjä, M. Kulmala, and N. Mihalopoulos (2015), Atmospheric new particle formation as a source of CCN in the eastern Mediterranean marine boundary layer, *Atmos. Chem. Phys.*, *15*(16), 9203–9215, doi:10.5194/acp-15-9203-2015.

Kawana, K., T. Nakayama, and M. Mochida (2016), Hygroscopicity and CCN activity of atmospheric aerosol particles and their relation to organics: Characteristics of urban aerosols in Nagoya, Japan, *J. Geophys. Res. Atmos.*, *121*, 4100–4121, doi:10.1002/2015JD023213.

King, S. M., T. Rosenoern, J. E. Shilling, Q. Chen, Z. Wang, G. Biskos, K. A. McKinney, U. Pöschl, and S. T. Martin (2010), Cloud droplet activation of mixed organic-sulfate particles produced by the photooxidation of isoprene, *Atmos. Chem. Phys.*, *10*(8), 3953–3964, doi:10.5194/acp-10-3953-2010.

Koehler, K. A., S. M. Kreidenweis, P. J. DeMott, A. J. Prenni, C. M. Carrico, B. Ervens, and G. Feingold (2006), Water activity and activation diameters from hygroscopicity data—Part II: Application to organic species, *Atmos. Chem. Phys.*, *6*(3), 795–809, doi:10.5194/acp-6-795-2006.

Laborde, M., et al. (2013), Black carbon physical properties and mixing state in the European megacity Paris, *Atmos. Chem. Phys.*, *13*(11), 5831–5856, doi:10.5194/acp-13-5831-2013.

Lee, S., Y. S. Ghim, S. W. Kim, and S. C. Yoon (2010), Effect of biomass burning and regional background aerosols on CCN activity derived from airborne in-situ measurements, *Atmos. Environ.*, *44*(39), 5227–5236, doi:10.1016/j.atmosenv.2010.08.044.

Li, Z., A. L. Williams, and M. J. Rood (1998), Influence of soluble surfactant properties on the activation of aerosol particles containing inorganic solute, *J. Atmos. Sci.*, *55*(10), 1859–1866, doi:10.1175/1520-0469(1998)055<1859:IOSSPO>2.0.CO;2.

McFiggans, G., et al. (2006), The effect of physical and chemical aerosol properties on warm cloud droplet activation, *Atmos. Chem. Phys.*, *6*(9), 2593–2649, doi:10.5194/acp-6-2593-2006.

Miyazaki, Y., Y. Kondo, N. Takegawa, Y. Komazaki, M. Fukuda, K. Kawamura, M. Mochida, K. Okuzawa, and R. J. Weber (2006), Time-resolved measurements of water-soluble organic carbon in Tokyo, *J. Geophys. Res.*, *111*, D22S30, doi:10.1029/2006JD007125.

Miyazaki, Y., S. G. Aggarwal, K. Singh, P. K. Gupta, and K. Kawamura (2009), Dicarboxylic acids and water-soluble organic carbon in aerosols in New Delhi, India, in winter: Characteristics and formation processes, *J. Geophys. Res.*, *114*, D19206, doi:10.1029/2009JD011790.

Miyazaki, Y., J. Jung, P. Fu, Y. Mizoguchi, K. Yamanoi, and K. Kawamura (2012), Evidence of formation of submicrometer water-soluble organic aerosols at a deciduous forest site in northern Japan in summer, *J. Geophys. Res.*, *117*, D19213, doi:10.1029/2012JD018250.

Mochida, M., M. Kuwata, T. Miyakawa, N. Takegawa, K. Kawamura, and Y. Kondo (2006), Relationship between hygroscopicity and cloud condensation nuclei activity for urban aerosols in Tokyo, *J. Geophys. Res.*, *111*, D23204, doi:10.1029/2005JD006980.

Mochida, M., C. Nishita-Hara, Y. Kitamori, S. G. Aggarwal, K. Kawamura, K. Miura, and A. Takami (2010), Size-segregated measurements of cloud condensation nucleus activity and hygroscopic growth for aerosols at Cape Hedo, Japan, in spring 2008, *J. Geophys. Res.*, *115*, D21207, doi:10.1029/2009JD013216.

Moore, R. H., A. Nenes, and J. Medina (2010), Scanning mobility CCN analysis—A method for fast measurements of size-resolved CCN distributions and activation kinetics, *Aerosol Sci. Technol.*, *44*(10), 861–871, doi:10.1080/02786826.2010.498715.

Orsini, D. A., Y. Ma, A. Sullivan, B. Sierau, K. Baumann, and R. J. Weber (2003), Refinements to the particle-into-liquid sampler (PILS) for ground and airborne measurements of water soluble aerosol composition, *Atmos. Environ.*, *37*(9–10), 1243–1259, doi:10.1016/S1352-2310(02)01015-4.

Padró, L. T., R. H. Moore, X. Zhang, N. Rastogi, R. J. Weber, and A. Nenes (2012), Mixing state and compositional effects on CCN activity and droplet growth kinetics of size-resolved CCN in an urban environment, *Atmos. Chem. Phys.*, *12*(21), 10,239–10,255, doi:10.5194/acp-12-10239-2012.

Paramonov, M., P. P. Aalto, A. Asmi, N. Prisle, V. M. Kerminen, M. Kulmala, and T. Petäjä (2013), The analysis of size-segregated cloud condensation nuclei counter (CCNC) data and its implications for cloud droplet activation, *Atmos. Chem. Phys.*, *13*(20), 10,285–10,301, doi:10.5194/acp-13-10285-2013.

Paramonov, M., et al. (2015), A synthesis of cloud condensation nuclei counter (CCNC) measurements within the EUCAARI network, *Atmos. Chem. Phys.*, *15*(21), 12,211–12,229, doi:10.5194/acp-15-12211-2015.

Pavuluri, C. M., K. Kawamura, M. Uchida, M. Kondo, and P. Fu (2013), Enhanced modern carbon and biogenic organic tracers in Northeast Asian aerosols during spring/summer, *J. Geophys. Res. Atmos.*, *118*, 2362–2371, doi:10.1002/jgrd.50244.

Peng, C., M. N. Chan, and C. K. Chan (2001), The hygroscopic properties of dicarboxylic and multifunctional acids: Measurements and UNIFAC predictions, *Environ. Sci. Technol.*, *35*(22), 4495–4501, doi:10.1021/es0107531.

Petters, M. D., and S. M. Kreidenweis (2007), A single parameter representation of hygroscopic growth and cloud condensation nucleus activity, *Atmos. Chem. Phys.*, *7*(8), 1961–1971, doi:10.5194/acp-7-1961-2007.

Pöschl, U., et al. (2010), Rainforest aerosols as biogenic nuclei of clouds and precipitation in the Amazon, *Science*, *329*(5998), 1513–1516, doi:10.1126/science.1191056.

Prenni, A. J., P. J. DeMott, S. M. Kreidenweis, D. E. Sherman, L. M. Russell, and Y. Ming (2001), The effects of low molecular weight dicarboxylic acids on cloud formation, *J. Phys. Chem. A*, *105*(50), 11,240–11,248, doi:10.1021/jp012427d.

Prenni, A. J., M. D. Petters, S. M. Kreidenweis, P. J. DeMott, and P. J. Ziemann (2007), Cloud droplet activation of secondary organic aerosol, *J. Geophys. Res.*, *112*, D10223, doi:10.1029/2006JD007963.

Renbaum-Wolff, L., M. Song, C. Marcolli, Y. Zhang, P. F. Liu, J. W. Grayson, F. M. Geiger, S. T. Martin, and A. K. Bertram (2016), Observations and implications of liquid–liquid phase separation at high relative humidities in secondary organic material produced by α-pinene ozonolysis without inorganic salts, *Atmos. Chem. Phys.*, *16*(12), 7969–7979, doi:10.5194/acp-16-7969-2016.

Roberts, G. C., and A. Nenes (2005), A continuous-flow streamwise thermal-gradient CCN chamber for atmospheric measurements, *Aerosol Sci. Technol.*, *39*(3), 206–221, doi:10.1080/027868290913988.

Roberts, G. C., D. A. Day, L. M. Russell, E. J. Dunlea, J. L. Jimenez, J. M. Tomlinson, D. R. Collins, Y. Shinozuka, and A. D. Clarke (2010), Characterization of particle cloud droplet activity and composition in the free troposphere and the boundary layer during INTEX-B, *Atmos. Chem. Phys.*, *10*(14), 6627–6644, doi:10.5194/acp-10-6627-2010.

Rood, M. J., and A. L. Williams (2001), Reply, *J. Atmos. Sci.*, *58*(11), 1468–1473, doi:10.1175/1520-0469(2001)058<1468:R>2.0.CO;2.

Rose, D., S. S. Gunthe, E. Mikhailov, G. P. Frank, U. Dusek, M. O. Andreae, and U. Pöschl (2008), Calibration and measurement uncertainties of a continuous-flow cloud condensation nuclei counter (DMT-CCNC): CCN activation of ammonium sulfate and sodium chloride aerosol particles in theory and experiment, *Atmos. Chem. Phys.*, *8*(5), 1153–1179, doi:10.5194/acp-8-1153-2008.

Saathoff, H., K.-H. Naumann, M. Schnaiter, W. Schöck, O. Möhler, U. Schurath, E. Weingartner, M. Gysel, and U. Baltensperger (2003), Coating of soot and $(NH_4)_2SO_4$ particles by ozonolysis products of α-pinene, *J. Aerosol Sci.*, *34*(10), 1297–1321, doi:10.1016/S0021-8502(03)00364-1.

Seinfeld, J. H., and S. N. Pandis (2006), *Atmospheric Chemistry and Physics: From Air Pollution to Climate Change*, 2nd ed., Wiley, New York.

Shingler, T., et al. (2016), Airborne characterization of subsaturated aerosol hygroscopicity and dry refractive index from the surface to 6.5 km during the SEAC4RS campaign, *J. Geophys. Res. Atmos.*, *121*, 4188–4210, doi:10.1002/2015JD024498.

Sihto, S.-L., et al. (2011), Seasonal variation of CCN concentrations and aerosol activation properties in boreal forest, *Atmos. Chem. Phys.*, *11*(24), 13,269–13,285, doi:10.5194/acp-11-13269-2011.

Silvergren, S., U. Wideqvist, J. Ström, S. Sjogren, and B. Svenningsson (2014), Hygroscopic growth and cloud forming potential of Arctic aerosol based on observed chemical and physical characteristics (a 1 year study 2007–2008), *J. Geophys. Res. Atmos.*, *119*, 14,080–14,097, doi:10.1002/2014JD021657.

Sorjamaa, R., B. Svenningsson, T. Raatikainen, S. Henning, M. Bilde, and A. Laaksonen (2004), The role of surfactants in Köhler theory reconsidered, *Atmos. Chem. Phys.*, *4*(8), 2107–2117, doi:10.5194/acp-4-2107-2004.

Suda, S. R., M. D. Petters, A. Matsunaga, R. C. Sullivan, P. J. Ziemann, and S. M. Kreidenweis (2012), Hygroscopicity frequency distributions of secondary organic aerosols, *J. Geophys. Res.*, *117*, D04207, doi:10.1029/2011JD016823.

Sun, J., and P. Ariya (2006), Atmospheric organic and bio-aerosols as cloud condensation nuclei (CCN): A review, *Atmos. Environ.*, *40*(5), 795–820, doi:10.1016/j.atmosenv.2005.05.052.

Swietlicki, E., et al. (2008), Hygroscopic properties of submicrometer atmospheric aerosol particles measured with H-TDMA instruments in various environments—A review, *Tellus Ser. B*, *60*, 432–469, doi:10.1111/j.1600-0889.2008.00350.x.

Varutbangkul, V., F. J. Brechtel, R. Bahreini, N. L. Ng, M. D. Keywood, J. H. Kroll, R. C. Flagan, J. H. Seinfeld, A. Lee, and A. H. Goldstein (2006), Hygroscopicity of secondary organic aerosols formed by oxidation of cycloalkenes, monoterpenes, sesquiterpenes, and related compounds, *Atmos. Chem. Phys.*, *6*(9), 2367–2388, doi:10.5194/acp-6-2367-2006.

Virkkula, A., R. Van Dingenen, F. Raes, and J. Hjorth (1999), Hygroscopic properties of aerosol formed by oxidation of limonene, α-pinene, and β-pinene, *J. Geophys. Res.*, *104*(D3), 3569–3579, doi:10.1029/1998JD100017.

Vlasenko, A., S. Sjögren, E. Weingartner, H. W. Gäggeler, and M. Ammann (2005), Generation of submicron Arizona test dust aerosol: Chemical and hygroscopic properties, *Aerosol Sci. Technol.*, *39*(5), 452–460, doi:10.1080/027868290959870.

Wang, H., K. Kawamura, and D. Shooter (2005), Carbonaceous and ionic components in wintertime atmospheric aerosols from two New Zealand cities: Implications for solid fuel combustion, *Atmos. Environ.*, *39*(32), 5865–5875, doi:10.1016/j.atmosenv.2005.06.031.

Weingartner, E., H. Burtscher, and U. Baltensperger (1997), Hygroscopic properties of carbon and diesel soot particles, *Atmos. Environ.*, *31*(15), 2311–2327, doi:10.1016/S1352-2310(97)00023-X.

Wex, H., F. Stratmann, D. Topping, and G. McFiggans (2008), The Kelvin versus the Raoult term in the Köhler equation, *J. Atmos. Sci.*, *65*(12), 4004–4016, doi:10.1175/2008JAS2720.1.

Whitehead, J. D., et al. (2016), Biogenic cloud nuclei in the central Amazon during the transition from wet to dry season, *Atmos. Chem. Phys.*, *16*(15), 9727–9743, doi:10.5194/acp-16-9727-2016.

Wise, M. E., J. D. Surratt, D. B. Curtis, J. E. Shilling, and M. A. Tolbert (2003), Hygroscopic growth of ammonium sulfate/dicarboxylic acids, *J. Geophys. Res.*, *108*(D20), 4638, doi:10.1029/2003JD003775.

Wu, Z. J., et al. (2013), Relating particle hygroscopicity and CCN activity to chemical composition during the HCCT-2010 field campaign, *Atmos. Chem. Phys.*, *13*(16), 7983–7996, doi:10.5194/acp-13-7983-2013.

Yttri, K. E., et al. (2007), Elemental and organic carbon in PM_{10}: A one year measurement campaign within the European Monitoring and Evaluation Programme EMEP, *Atmos. Chem. Phys.*, *7*(22), 5711–5725, doi:10.5194/acp-7-5711-2007.